2016 IEEE International Conference on Robotics and Automation (ICRA)
Stockholm, Sweden, May 16-21, 2016

Essential considerations for design and control of human-interactive robots

Hyunglae Lee, *Member* and Neville Hogan, *Member*

***Abstract*—Managing the trade-off between performance and stability is a crucial issue in physical human-robot interaction, and this has become more important than ever apace with growing needs for physically human-interactive robots in many fields, such as assistive robotics and rehabilitation robotics. In this paper, we present two essential considerations for design and control of robots physically interacting with humans: *energetic passivity* and *mechanical impedance*. Characterization of passive, dissipative, and active behavior of the human neuromuscular system is essential to ensure and control coupled stability in physical human-robot interaction. In addition, characterization of human mechanical impedance at the interaction port provides detailed quantitative information to describe interactive dynamics. The importance of these characterizations is demonstrated by simple examples and the authors' previous research on the human ankle. Implications for quantitative guidelines for robot design and control are discussed.**

I. Introduction

The demand for advanced physical human-robot interaction has grown in many fields, with clinical, industrial, and military applications. For example, a number of robotic exoskeletons have recently been introduced and commercialized to assist and rehabilitate patients having neurological impairments [1-3]. In addition, there have been significant recent advances in active prosthetic devices to restore amputees' motor functions [4-6]. In industrial and military applications, robotic devices have been utilized mainly to augment human strength and endurance [7-9].

One essential requirement in all of the above applications in which robots operate in close physical contact with humans is to achieve coupled stability and at the same time maximize performance. In fact, managing the trade-off between stability and performance has been a very important issue throughout the history of physical human-robot interaction [10-13].

Manuscript received September 15, 2015. This work was supported by Toyota Motor Corporation, The Gloria Blake Fund, and the Eric P. and Evelyn E. Newman Fund. Hyunglae Lee was supported in part by a Samsung Scholarship. N. Hogan is a co-inventor in the MIT-held patent for the robotic device used in this work. He holds equity positions in Interactive Motion Technologies, the company that manufactures this type of technology under license to MIT.

Hyunglae Lee is with the School for Engineering of Matter, Transport, and Energy, Arizona State University, AZ 85287 USA (corresponding author, phone: 617-548-5106; e-mail: hyunglae.lee@asu.edu).

Neville Hogan is with the Mechanical Engineering Department, and Brain and Cognitive Science Department, Massachusetts Institute of Technology, MA 02139 USA (e-mail: neville@mit.edu).

On the robot side, better mechanical design and innovation in actuator technologies, such as actuators capable of expressing high force density and low mechanical impedance, could be advantageous to improve the trade-off. On the other hand, on the human side, there still remains room to improve the trade-off with better understanding of human neuromuscular behavior that can be incorporated in the design of robotic controllers. In an effort to better characterize human behavior, "first-principles" models of human dynamics, analogous to the Lagrangian dynamics of a robot, have been widely used [14, 15]. While multibody musculoskeletal simulations provide valuable quantitative information predicting human behaviors in a wide range of dynamic tasks and enable simulation-based design of robotic systems [16], they have inevitable limitations arising due to model uncertainties and errors in simulation parameters [17].

To address these challenges we characterized the dynamics seen at the points of contact, i.e., "interaction ports", where two-way energy exchange occurs between the human and the robot. More specifically, we quantified energetic passivity/non-passivity and mechanical impedance at the interaction port. In this paper, we describe why these are essential considerations for design and control of human-interactive robots. The importance of this characterization is demonstrated by simple examples and the authors' previous research on the human ankle. Implications for mechanical design and controller implementation are discussed.

II. Energetic Passivity

Energetic passivity, describing how a system, for any time period, cannot output more energy than what is stored in it, is a central concept to explain and ensure coupled stability in physical human-robot interaction. It is known that necessary and sufficient conditions for a system to be stable when coupled to any stable and passive object is that its driving point impedance should be energetically passive [12].

Most physical environments that robots interact with are passive. Any combination of passive mechanical elements (springs, dampers, inertia), whether linear or non-linear, is energetically passive. However, there is no a priori justification to assume that human limbs and joints are fundamentally passive. Just as feedback delays usually compromise passivity as well as stability in robot controls, significant delays in human neural feedback due to limited nerve conduction velocity (less than 120 m/s even in the

fastest myelinated neurons [18]) may act as a source of non-passivity.

In fact, several previous studies have demonstrated that human neuromuscular system can exhibit significant non-passive behavior [19, 20], and it is known that non-passivity of the neuromuscular system is clearly associated with reflex actions, which are highly modifiable [21].

Non-passivity of the human neuromuscular system, more specifically active behavior, may function as an energy source and consequently affect coupled stability as well as performance in physical human-robot interaction. Thus, it is essential to characterize passivity/non-passivity of the human limbs/joints at the interaction port. Note that the passivity/non-passivity of interactive behavior is distinct from the ability of a system to generate positive work. Instead, it describes the generation of mechanical work, either positive or negative, solely based upon motion at the interaction port(s).

Curl analysis and passivity analysis enable the quantitative characterization of energetic passivity/non-passivity in static and dynamic conditions, respectively.

A. Curl Analysis

Curl analysis based on vector field approximation provides a quantification of the extent to which the neuromuscular system is energetically passive or non-passive [22]. For example, consider a neuromuscular system physically interacting with a robot in a 2-D space. A vector field ($\boldsymbol{V}$), possibly non-linear, is defined to relate displacements/angular displacements ($\boldsymbol{r}$) to forces/torques ($\boldsymbol{F}$) at the interaction port (Eq. (1)):

$$(F_1, F_2) = \boldsymbol{V}(r_1, r_2) \tag{1}$$

where subscripts 1 and 2 denote axes defining the coordinate system at the interaction port. The continuous field can be precisely approximated based on thin-plate spline smoothing [23] and generalized cross validation [24].

While the vector field accurately describes the non-linear relationship between displacements and forces over the entire measured task space, a stiffness matrix ($\boldsymbol{K}$) can be defined at any point in the displacement field by linearly approximating the relationship between the imposed displacements ($\delta\boldsymbol{r}$) and the resulting forces ($\delta\boldsymbol{F}$) (Eq. (2)):

$$\delta\boldsymbol{F} = -\boldsymbol{K}\delta\boldsymbol{r}$$

$$\begin{bmatrix}\delta F_1\\ \delta F_2\end{bmatrix} = \begin{bmatrix}\partial F_1/\partial r_1 & \partial F_1/\partial r_2\\ \partial F_2/\partial r_1 & \partial F_2/\partial r_2\end{bmatrix}\begin{bmatrix}\delta r_1\\ \delta r_2\end{bmatrix} \tag{2}$$

Each element of the stiffness matrix ($\boldsymbol{K}$) can be directly calculated by differentiating the smoothly approximated (satisfying C1 continuity [22, 23]) nonlinear field ($\boldsymbol{V}$).

The stiffness matrix ($\boldsymbol{K}$) is further decomposed into symmetric ($\boldsymbol{K_s} = (\boldsymbol{K}+\boldsymbol{K}^T)/2$) and anti-symmetric ($\boldsymbol{K_a} = (\boldsymbol{K}-\boldsymbol{K}^T)/2$) components [21]. The anti-symmetric component, or the curl (rotational) component, is non-passive since

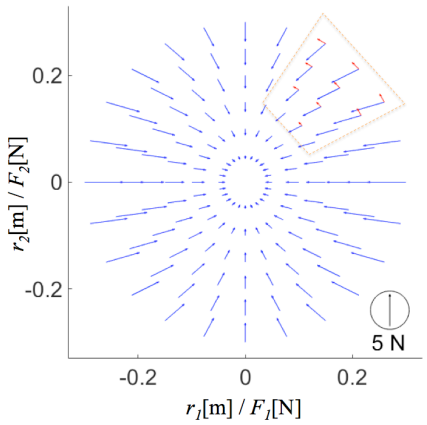

Fig.1. Decomposition of the vector field into a conservative field (blue) and a rotational field (red). The force is illustrated by an arrow with its tail at the tip of the displacement vector. Note that non-zero curl exists only in the region where anti-symmetric stiffness ($\boldsymbol{K_L}$) constitutes the vector field (the highlighted region). $\sqrt{K_{ratio}}$ in the region of non-zero curl is 35.4%.

cyclic displacements may add or remove energy. Thus, we can quantify the level of passivity/non-passivity of the neuromuscular system by comparing the relative size of $\boldsymbol{K_s}$ and $\boldsymbol{K_a}$ (Eq. (3)):

$$\sqrt{K_{ratio}} = \sqrt{\det(\boldsymbol{K_a})} / \sqrt{\det(\boldsymbol{K_s})} \times 100 \tag{3}$$

Apparently, zero-curl ($\boldsymbol{K_a}=\boldsymbol{0_{2,2}}$) leads to $\sqrt{K_{ratio}} = 0$, where the system exhibits perfectly passive behavior.

As a simple example, suppose that the relationship between the imposed displacements and the corresponding forces at the interaction port is defined by the following two stiffness matrices ($\boldsymbol{K_G}$ and $\boldsymbol{K_L}$):

$$\boldsymbol{K_G} = \begin{bmatrix}20 & 0\\ 0 & 10\end{bmatrix}[N/m], \quad -0.3 \le r_1, r_2 \le 0.3[m] \text{ except } \boldsymbol{K_L} \text{ region}$$

$$\boldsymbol{K_L} = \begin{bmatrix}20 & 5\\ -5 & 10\end{bmatrix}[N/m], \quad 0.1 \le r_1, r_2 \le 0.3[m]$$

The anti-symmetric matrix $\boldsymbol{K_L}$ is defined to simulate unbalanced inter-muscular feedback at the interaction port. When the vector field defined by $\boldsymbol{K_G}$ and $\boldsymbol{K_L}$ is decomposed into a conservative and a rotational field, it is clear that anti-symmetric stiffness manifests as non-zero curl in the rotational field (Fig. 1). In this example, cyclic counter-clockwise motion in the region of $\boldsymbol{K_L}$ will continuously add energy at the interaction port and hence weaken coupled stability.

B. Passivity Analysis

While curl analysis characterizes static behavior of the neuromuscular system, passivity analysis quantifies passive, dissipative, and active behavior at the interaction port over a wide range of frequencies [25].

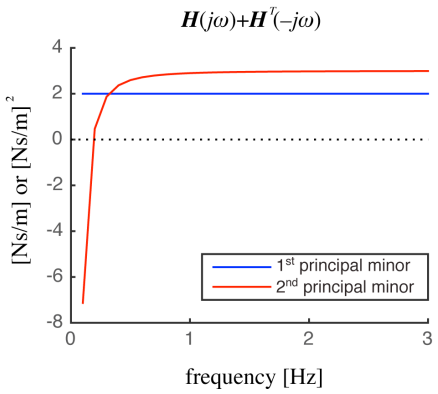

Fig. 2. Passivity analysis for the simple example. The first and the second leading principal minors of the matrix $\boldsymbol{H}(jw)+\boldsymbol{H}^T(-jw)$ are presented.

For the linear time-invariant case, the passivity formulation for a *n*-port system is as Eq. (4) [12, 26]:

$$\forall \omega \geq 0,\ \boldsymbol{H}(j\omega)+\boldsymbol{H}^T(-j\omega) \geq 0 \qquad (4)$$
$$\boldsymbol{y}(j\omega) = \boldsymbol{H}(j\omega)\boldsymbol{u}(j\omega)$$

where j is the complex operator, the superscript T is the transpose operator, and ω denotes frequency. $\boldsymbol{H}$ is a transfer matrix relating inputs ($\boldsymbol{u}$) and outputs ($\boldsymbol{y}$) to the system, where $\boldsymbol{u}$ and $\boldsymbol{y}$ are power conjugate variables that define power flow ($P_{in}=\boldsymbol{u}^T\boldsymbol{y}$) into the system. If equality is restricted from Eq. (4), the system is dissipative. Furthermore, when $\boldsymbol{H}(j\omega)+\boldsymbol{H}^T(-j\omega)<0$ for any frequency, the system is active, which means that it delivers more energy than what is delivered to it.

As a simple example, suppose that the transfer matrix $\boldsymbol{H}$ relating input velocities ($\boldsymbol{u}=\boldsymbol{v}$) and the corresponding forces ($\boldsymbol{y}=\boldsymbol{f}$) at the interaction port is defined as follow, where s is the Laplace operator:

$$\boldsymbol{y}(s) = \boldsymbol{H}(s)\boldsymbol{u}(s)$$
$$\boldsymbol{H}(s) = \begin{bmatrix} 1+20/s & 0.5+5/s \\ 0.5+3/s & 1+20/s \end{bmatrix} [Ns/m]$$

Anti-symmetric stiffness and symmetric damping are combined and simulated. Positive semi-definiteness/positive definiteness of the 2-by-2 matrix $\boldsymbol{H}(j\omega)+\boldsymbol{H}^T(-j\omega)$ is assessed by evaluating all of the leading principal minors of the matrix. Apparently, the first leading principal minor is positive at all frequencies. The second leading principal minor, the determinant of $\boldsymbol{H}$, varies with frequency (Fig. 2). In the low frequency region, below about 0.2 Hz where stiffness dominates the system response, the determinant of $\boldsymbol{H}$ is negative. This active behavior is due to anti-symmetric stiffness as observed in the example of curl analysis. In higher frequencies where damping dominates the response, the determinant value is positive, implying that the system is dissipative. Thus, passivity analysis enables characterization of the extent to which the port behavior is passive, dissipative, or active over the frequency.

III. Mechanical Impedance

Human mechanical impedance, which describes the relationship between joint/limb displacement and the corresponding force during a perturbation, is another essential concept to consider in designing and controlling human-interactive robots. It is a fundamental property of the human neuromuscular system that facilitates seamless, dynamic interactions with the physical environment. As mechanical impedance may be quite different between individuals, it is important to accurately quantify this property, and the robot should incorporate this to improve its performance in interaction with humans. Here we describe a set of characterization methods to quantify multivariable human mechanical impedance, applicable to any multi-joint system or single joint having multiple DOFs.

A. Static Mechanical Impedance

The static component of mechanical impedance is a force-displacement (or torque-angular displacement) relationship at the interaction port (Eq. (1)), and can be precisely characterized by the non-linear vector field approximation method described in the section II.A.

As the field defining static mechanical impedance is continuous over the entire measured task space, we can calculate the directional variation of static mechanical impedance at any given nominal point in the displacement field. More specifically, the effective stiffness for each movement direction is calculated by computing the slope of a least squares fit to the displacement (angular displacement) and force (torque) data in that direction. Results in all movement directions can be visualized in a multi-dimensional space. For example, in the 2-DOF case, results can be plotted in polar coordinates, where the angle and radius correspond to each movement direction in 2-D space and the magnitude of effective stiffness in that direction, respectively.

While this method quantifies non-linear behavior of the neuromuscular system over a wide range of motions, it is only limited to the static component of the mechanical impedance, and cannot provide information on higher order dynamics.

B. Dynamic Mechanical Impedance

Dynamic mechanical impedance quantifies the characteristics of the neuromuscular system as a function of frequency, which complements the limitation of static mechanical impedance.

Multivariable dynamic mechanical impedance can be estimated by various multi-input multi-output system

identification methods. Among them, non-parametric linear stochastic system identification is preferred. First, the use of random white noise minimizes the likelihood of voluntary reactions of human subjects. Second, the non-parametric approach requires no a-priori assumption about the structure of the neuromuscular system.

Estimation results for axes defining the coordinate system are represented either by a frequency response matrix or an impulse response matrix, depending on the method used [27]. In addition, with coordinate transformations, we can estimate the directional variation of mechanical impedance as described in the previous section, but now as a function of frequency. Estimation of multivariable mechanical impedance is not limited to time-invariant cases, but can be extended to time-varying dynamic task conditions [28].

One limitation of this method is that multiple measurements with different nominal points are required to characterize impedance over a wide range of motions.

Note that each method to characterize static and dynamic mechanical impedance has its own advantages and limitations; and they complement each other. Hence, a combination of them using the same experimental setup provides more elaborate characterization of the human neuromuscular system in various task conditions.

IV. Case Study: Unimpaired Human Ankle

This section presents a case study based on a series of our previous work on the human ankle [29, 30]. The human ankle plays critical roles in stabilizing and controlling the lower limb during interaction with the surrounding physical environments. For example, the ankle contributes to postural balance control during standing, and propulsion, shock absorption, and lower limb coordination during locomotion. Given its significance, we have characterized energetic passivity/non-passivity and mechanical impedance of the unimpaired ankle using the methods described in the previous sections. A brief summary of this research with 10 young unimpaired individuals is provided below.

A wearable ankle robot, Anklebot (Interactive Motion Technologies Inc., Watertown, MA) [31], was utilized as a centerpiece of the study. The robot has very low intrinsic mechanical impedance, allowing human subjects to move the ankle with minimal resistance, i.e., it is highly back drivable. It allows normal range of motion in all 3 degrees-of-freedom (DOFs) of the foot and actuates its 2 DOFs including inversion-eversion (IE) and dorsiflexion-plantarflexion (DP) motions (Fig. 3A).

For curl analysis, the torque-angle relationship at the ankle in 2 DOFs (IE−DP) was measured under different muscle activation conditions; fully relaxed, tibialis anterior (TA) active, soleus (SOL) active, and co-contraction of both TA and SOL. The target activation level was set as 10% of the maximum voluntary contraction (MVC) of each muscle. A simple impedance controller (proportional gain: 200

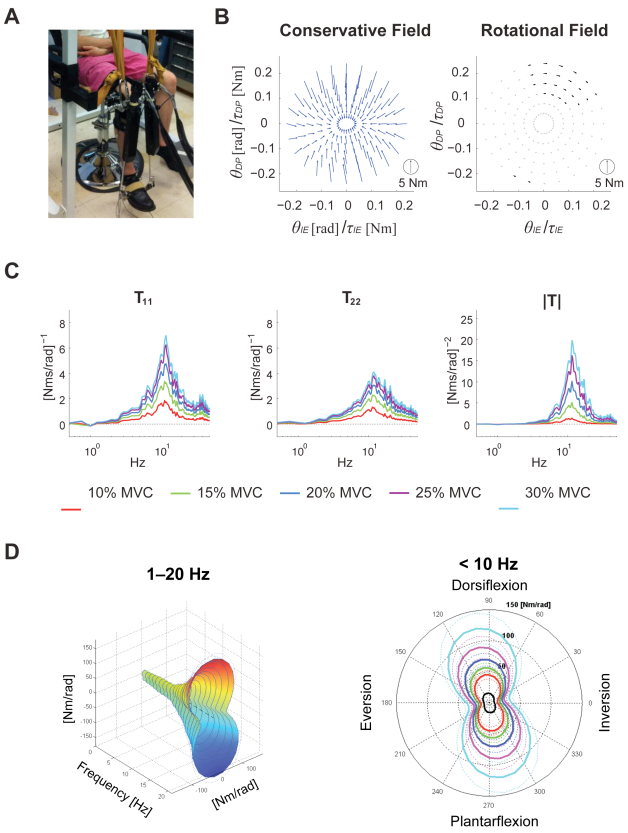

Fig. 3. Representative results from the ankle study. **A**: The robot was attached to the knee brace and the custom designed shoe. Measurements were performed in the seated posture. **B**: An example from the curl analysis (SOL active study). Black lines in the rotational field denote statistically significant non-zero curl. **C**: Group results from the passivity analysis (SOL active study). Diagonal elements and the determinant of $\boldsymbol{T}(jw) = \boldsymbol{H}(jw) + \boldsymbol{H}^{T}(-jw)$ are presented. **D**: (Left) Directional variation of ankle mechanical impedance as a function of frequency (1~20 Hz) in fully relaxed muscles. (Right) Directional variation of ankle mechanical impedance (averaged below 10 Hz) with SOL active [30].

Nm/rad; derivative gain 1 Nms/rad) was used to deliver quasi-static (10°/s) ramp perturbations to the 2 DOFs of the ankle with nominal displacement amplitude of 15°.

When muscles were fully relaxed, curls in the rotational field were statistically indistinguishable from zero [22]. When muscles were active, either unilaterally or antagonistically, statistically non-zero curls were observed in some regions of the rotational field (Fig. 3B). However, this non-passive behavior was modest in the young unimpaired subjects we studied. It was evidenced by the observation that a large portion of the curls in the rotational field fell within the zero-curl criterion. Furthermore, calculation of $\sqrt{K_{ratio}}$ showed that the anti-symmetric parts of the stiffness matrix ($\boldsymbol{K_a}$) were substantially smaller than its symmetric parts ($\boldsymbol{K_s}$) (Table. 1).

For passivity analysis, inputs ($\boldsymbol{u}$) and outputs ($\boldsymbol{y}$) at the interaction port were selected as torques and angular velocities in coordinates (IE′−DP′), defined by rotating the original joint coordinates (IE−DP) by 45° counter-

TABLE I. RELATIVE SIZE OF NON-PASSIVE ELEMENTS TO THE PASSIVE ELEMENTS [%]

$\sqrt{K_{ratio}}$ in curl analysis			
TA active	SOL Active	Co-contraction	
11.5 (2.0)	13.7 (3.2)	11.3 (3.4)	
$\sqrt{Z_{ratio}}$ in passivity analysis			
	10% MVC	15% MVC	20% MVC	25% MVC	30% MVC
TA active	7.9 (4.5)	7.7 (4.0)	3.8 (1.6)	5.8 (4.5)	5.4 (2.4)
SOL active	10.0 (6.6)	6.6 (4.6)	6.9 (5.4)	6.6 (4.9)	6.3 (4.7)

Mean and standard deviation (in parentheses) of 10 subjects are presented.

clockwise: $\boldsymbol{u} = \boldsymbol{\tau}' = (\tau_{IE'}, \tau_{DP'})$ and $\boldsymbol{y} = \boldsymbol{\omega}' = (\omega_{IE'}, \omega_{DP'})$. The study was performed under different muscle activation conditions; fully relaxed and different target levels of TA and SOL activity, from 10% to 30% MVC with increments of 5% MVC. To calculate the transfer matrix ($\boldsymbol{H}$) relating input torques and the corresponding output angular velocities, linear time-invariant multi-input multi-output system identification methods were used [27]. A simple impedance controller with a proportional gain (37.2 and 76.0 Nm/rad for IE and DP directions, respectively) was combined with mild random torque perturbations to excite the ankle while holding it around its initial position against active ankle torques [30].

Active behavior of the ankle was modest over a wide range of frequency (Fig. 3C). In the low-frequency region below about 2 Hz where stiffness dominates, the ankle behavior was close to passive ($\boldsymbol{H}(j\omega) + \boldsymbol{H}^T(-j\omega) \approx 0$). Only a few subjects (one in the TA active study and three in the SOL active study) exhibited active behavior. The relative size of the anti-symmetric and symmetric parts of the impedance matrix ($\boldsymbol{Z}(s) = \boldsymbol{\tau}'(s) / \boldsymbol{\theta}'(s)$) was calculated similarly as Eq. (3) ($\sqrt{Z_{ratio}}$). When averaged below 2 Hz, it was less than 10% (Table. 1). In the frequency region above about 3 Hz up to 10–20 Hz, the ankle behavior gradually changed to dissipative ($\boldsymbol{H}(j\omega) + \boldsymbol{H}^T(-j\omega) > 0$), indicating that this region was dominated by ankle viscosity. Dissipative behavior weakened gradually at higher frequencies as inertia became predominant.

Static and dynamic ankle mechanical impedances were estimated from the same data sets for curl analysis and passivity analysis, respectively. One major finding is that both static and dynamic ankle impedances of young impaired subjects were strongly direction dependent. Ankle mechanical impedance was weaker in IE than DP direction, resulting in a characteristic "peanut" shape structure over a wide range of frequencies [32]. When muscles were active, either unilaterally or antagonistically, ankle mechanical impedance increased in all movement directions in the IE–DP space, but impedance increased more in DP than IE direction, accentuating the characteristic "peanut" structure (Fig. 3D) [30].

V. DISCUSSION: IMPLICATIONS FOR DESIGN AND CONTROL OF HUMAN-INTERACTIVE ROBOTS

How could quantitative characterization of energetic passivity and mechanical impedance be utilized to improve the trade-off between stability and performance in physical human robot interaction?

Characterization of energetic passivity provides a guideline to adjust mechanical impedance of a robot at the interaction port. If a human subject interacting with a robot exhibits highly dissipative behavior, designing a robot controller to achieve passive driving point impedance might be unnecessarily conservative and hence limit performance. To better utilize the robot's performance, less conservative approaches may be chosen by controlling the robot's mechanical impedance to be active while still maintaining robust coupled stability. For example, our work demonstrated that the ankle of healthy young humans is predominantly passive and dissipative over a wide range of frequency. This suggests that lower-extremity robotic devices in industrial and military applications, where high performance matters, may be controlled with less conservative control strategies without compromising coupled stability.

On the other hand, if the human subject exhibits energetically active behavior, the robot should compensate this by being strongly dissipative to secure coupled stability. In fact, we may expect significantly active behavior from neurologically impaired individuals, who are potential beneficiaries of assistive and/or rehabilitation robots. For example, previous studies have demonstrated that both intrinsic and reflexive properties of the impaired ankle are significantly different from those of unimpaired subjects. It is probable that the damage to central and peripheral neural networks following impairments, such as stroke [33, 34], multiple sclerosis [35], and spinal cord injury [36] alters reflex feedback. At the early stage of rehabilitation, it is desirable to design the robot to be strongly dissipative to cope with the patient's active behavior. As the patient recovers and the degree of non-passivity improves, the robot's dissipativity could be modulated as needed.

Another application of quantitative information about energetic passivity is human motor control and learning. Adaptation strategies similar to those introduced for rehabilitation might apply to unimpaired subjects as they initially learn how to operate robotic devices such as exo-skeletons: start with the robot dissipative; progressively adapt towards passive; and maybe to non-passive if it provides performance benefits.

Characterization of mechanical impedance further provides a quantitative guideline to optimize the trade-off between stability and performance. For example, loop-shaping algorithms based on complementary stability outperform passivity-based controllers [37]. This algorithm

incorporates limited knowledge of environments to improve performance. Better characterization of the human neuromuscular system is expected to provide more accurate information on the environment that the robot interacts with, and may further improve performance while still guaranteeing coupled stability.

Refined characterization of mechanical impedance is also beneficial to robot design. By incorporating information on the directional variation of mechanical impedance, we can optimize mechanical design, e.g. inertia distribution, as well as actuator selection. For example, highly directional information about the ankle being weakest in IE direction informs that an ankle robot is desired to have higher torque capacity in the sagittal plane than in the frontal plane.

In summary, characterization of energetic passivity and mechanical impedance provides quantitative guidelines to optimize mechanical design and control strategies to maximize performance and secure coupled stability at the same time. In such a way, this study may facilitate further innovation in physically interactive robots in many fields including assistive robotics and rehabilitation robotics.

REFERENCES

[1] EksoBionics, "http://www.eksobionics.com/ekso."

[2] ReWalk, "rewalk.com."

[3] H. A. Quintero, R. J. Farris, and M. Goldfarb, "A Method for the Autonomous Control of Lower Limb Exoskeletons for Persons With Paraplegia," *Journal of Medical Devices-Transactions of the Asme,* vol. 6, Dec 2012.

[4] L. J. Hargrove, A. M. Simon, A. J. Young, R. D. Lipschutz, S. B. Finucane, D. G. Smith*, et al.*, "Robotic Leg Control with EMG Decoding in an Amputee with Nerve Transfers," *New England Journal of Medicine,* vol. 369, pp. 1237-1242, Sep 26 2013.

[5] F. Sup, A. Bohara, and M. Goldfarb, "Design and control of a powered transfemoral prosthesis," *International Journal of Robotics Research,* vol. 27, pp. 263-273, Feb 2008.

[6] S. K. Au and H. M. Herr, "Powered ankle-foot prosthesis - The importance of series and parallel motor elasticity," *IEEE Robotics & Automation Magazine,* vol. 15, pp. 52-59, Sep 2008.

[7] Sarcos, "http://www.sarcos.com/."

[8] LockheedMartin, " http://www.lockheedmartin.com/products/hulc."

[9] H. Kawamoto and Y. Sankai, "Power Assist System HAL-3 for Gait Disorder Person," *In Proc. International Conference Computers Helping People with Special Needs (Lecture Note in Computer Science),* vol. 2398, pp. 196-203, 2002.

[10] W. S. Newman, "Stability and Performance Limits of Interaction Controllers," *Journal of Dynamic Systems Measurement and Control-Transactions of the Asme,* vol. 114, pp. 563-570, Dec 1992.

[11] N. Hogan and S. P. Buerger, "Impedance and interaction control," *Robotics and Automation Handbook, New York, CRC Press,* 2005.

[12] J. E. Colgate and N. Hogan, "Robust-Control of Dynamically Interacting Systems," *International Journal of Control,* vol. 48, pp. 65-88, Jul 1988.

[13] H. Kazerooni, "Human Robot Interaction Via the Transfer of Power and Information Signals," *Ieee Transactions on Systems Man and Cybernetics,* vol. 20, pp. 450-463, Mar-Apr 1990.

[14] S. L. Delp, F. C. Anderson, A. S. Arnold, P. Loan, A. Habib, C. T. John*, et al.*, "OpenSim: open-source software to create and analyze dynamic Simulations of movement," *Ieee Transactions on Biomedical Engineering,* vol. 54, pp. 1940-1950, Nov 2007.

[15] M. Damsgaard, J. Rasmussen, S. T. Christensen, E. Surma, and M. de Zee, "Analysis of musculoskeletal systems in the AnyBody Modeling System," *Simulation Modelling Practice and Theory,* vol. 14, pp. 1100-1111, Nov 2006.

[16] C. Ong, J. Hicks, and S. L. Delp, "Simulation-Based Design for Wearable Robotic Systems: An Optimization Framework for Enhancing a Standing Long Jump," *IEEE Trans Biomedical Engineering,* 2015.

[17] M. E. Lund, M. de Zee, M. S. Andersen, and J. Rasmussen, "On validation of multibody musculoskeletal models," *Proceedings of the Institution of Mechanical Engineers Part H-Journal of Engineering in Medicine,* vol. 226, pp. 82-94, 2012.

[18] A. Siegel, H. N. Sapru, and H. Siegel, *Essential neuroscience*, Third edition. ed.

[19] F. Lacquaniti, M. Carrozzo, and N. A. Borghese, "Time-varying mechanical behavior of multijointed arm in man," *J Neurophysiol,* vol. 69, pp. 1443-64, May 1993.

[20] H. Gomi and M. Kawato, "Human arm stiffness and equilibrium-point trajectory during multi-joint movement," *Biological Cybernetics,* vol. 76, pp. 163-71, Mar 1997.

[21] N. Hogan, "The Mechanics of Multi-Joint Posture and Movement Control," *Biological Cybernetics,* vol. 52, pp. 315-331, 1985.

[22] H. Lee, P. Ho, M. A. Rastgaar, H. I. Krebs, and N. Hogan, "Multivariable static ankle mechanical impedance with relaxed muscles," *Journal of Biomechanics,* vol. 44, pp. 1901-1908, Jul 7 2011.

[23] F. L. Bookstein, "Principal Warps - Thin-Plate Splines and the Decomposition of Deformations," *IEEE Transactions on Pattern Analysis and Machine Intelligence,* vol. 11, pp. 567-585, Jun 1989.

[24] G. Wahba, *Spline models for observational data*. Philadelphia, Pa.: Society for Industrial and Applied Mathematics, 1990.

[25] E. Colgate, "The Control of Dynamically Interacting Systems " *PhD Dissertation at the Massachusetts Institute of Technology (MIT),* 1988.

[26] J. J. E. Slotine and W. Li, *Applied nonlinear control*. Englewood Cliffs, N.J.: Prentice Hall, 1991.

[27] E. J. Perreault, R. F. Kirsch, and A. M. Acosta, "Multiple-input, multiple-output system identification for characterization of limb stiffness dynamics," *Biological Cybernetics,* vol. 80, pp. 327-337, May 1999.

[28] J. B. Macneil, R. E. Kearney, and I. W. Hunter, "Identification of Time-Varying Biological-Systems from Ensemble Data," *IEEE Transactions on Biomedical Engineering,* vol. 39, pp. 1213-1225, Dec 1992.

[29] H. Lee, P. Ho, M. Rastgaar, H. I. Krebs, and N. Hogan, "Multivariable Static Ankle Mechanical Impedance with Active Muscles," *IEEE Transactions on Neural Systems and Rehabilitation Engineering,* vol. 22, pp. 44-52, Jan 2014.

[30] H. Lee, H. I. Krebs, and N. Hogan, "Multivariable Dynamic Ankle Mechanical Impedance with Active Muscles," *IEEE Transactions on Neural Systems and Rehabilitation Engineering,* vol. 22, pp. 971-981, Sep 2014.

[31] A. Roy, H. I. Krebs, D. J. Williams, C. T. Bever, L. W. Forrester, R. M. Macko*, et al.*, "Robot-Aided Neurorehabilitation: A Novel Robot for Ankle Rehabilitation," *IEEE Transactions on Robotics,* vol. 25, pp. 569-582, Jun 2009.

[32] H. Lee, H. I. Krebs, and N. Hogan, "Multivariable Dynamic Ankle Mechanical Impedance with Relaxed Muscles," *IEEE Transactions on Neural Systems and Rehabilitation Engineering,* vol. 22, pp. 1104-1114, Nov 2014.

[33] S. G. Chung, E. van Rey, Z. Q. Bai, E. J. Roth, and L. Q. Zhang, "Biomechanic changes in passive properties of hemiplegic ankles with spastic hypertonia," *Archives of Physical Medicine and Rehabilitation,* vol. 85, pp. 1638-1646, Oct 2004.

[34] H. Lee, T. Patterson, J. Ahn, D. Klenk, A. Lo, H. I. Krebs*, et al.*, "Static Ankle Impedance in Stroke and Multiple Sclerosis: A Feasibility Study," *2011 Annual International Conference of the IEEE Engineering in Medicine and Biology Society (EMBC),* pp. 8523-8526, 2011.

[35] T. Sinkjaer, E. Toft, K. Larsen, S. Andreassen, and H. J. Hansen, "Nonreflex and Reflex Mediated Ankle Joint Stiffness in Multiple-Sclerosis Patients with Spasticity," *Muscle & Nerve,* vol. 16, pp. 69-76, Jan 1993.

[36] M. M. Mirbagheri, H. Barbeau, M. Ladouceur, and R. E. Kearney, "Intrinsic and reflex stiffness in normal and spastic, spinal cord injured subjects," *Exp Brain Res,* vol. 141, pp. 446-59, Dec 2001.

[37] S. P. Buerger and N. Hogan, "Complementary stability and loop shaping for improved human-robot interaction," *IEEE Transactions on Robotics,* vol. 23, pp. 232-244, Apr 2007.